Exfoliated graphene sheets decorated with metal / metal oxide nanoparticles: simple preparation from cation exchanged graphite oxide

Kazuma Gotoh [a], Taro Kinumoto [b], Eiji Fujii [c], Aki Yamamoto [a], Hideki Hashimoto [a], Takahiro Ohkubo [a], Atsushi Itadani [a], Yasushige Kuroda [a], and Hiroyuki Ishida [a]*

[a] Graduate School of Natural Science & Technology, Okayama University, 3-1-1 Tsushima-naka, Okayama 700-8530, Japan

[b] Faculty of Engineering, Oita University, 700 Dannoharu, Oita 870-1192, Japan

[c] New Materials Group, Industrial Technology Center of Okayama Prefecture, 5301 Haga, Okayama 701-1296, Japan

Abstract

We produced carbon hybrid materials of graphene sheets decorated with metal or metal oxide nanoparticles of gold, silver, copper, cobalt, or nickel from cation exchanged graphite oxide. Measurements using powder X-ray diffraction, transmission electron microscopy, and X-ray absorption spectra revealed that the Au and Ag in the materials (Au–Gr and Ag–Gr) existed on graphene sheets as metal nanoparticles, whereas Cu and Co in the materials (Cu–Gr and Co–Gr) existed as a metal oxide. Most Ni particles in Ni–Gr were metal, but the surfaces of large particles were partly oxidized, producing a

*Corresponding author. Tel/Fax: +81 86 251 7776

E-mail address: kgotoh@cc.okayama-u.ac.jp (K. Gotoh)

core–shell structure. The Ag–Gr sample showed a catalytic activity for the oxygen reduction reaction in 1.0 M KOH aq. under an oxygen atmosphere. Ag–Gr is superior as a cathode in alkaline fuel cells, which should not be disturbed by the methanol cross-over problem from the anode. We established an effective approach to prepare a series of graphene-nanoparticle composite materials using heat treatment.

1. Introduction

Graphene materials [1, 2] and graphene-derived materials such as graphene oxide [3-5] and exfoliated graphene sheets [6-8] have attracted much attention because of their structural and electrical properties [9-11]. These new carbon materials also offer sufficient area to support metal nanoparticles. They can achieve higher catalyst utility than those using conventional porous carbon materials. Actually, some graphene-based materials having metallic nanoparticles such as TiO_2 [12, 13], ZnO, Au, and Pt [14-19] have been synthesized from dispersed graphene oxide or exfoliated graphene sheets using impregnation method, sol–gel method, and others.

Some carbon materials produced from graphene sheets have been created from intercalation compounds of graphite oxide and hydrophilic intercalants (some metallic precursors) through exfoliation during calcination procedures or chemical reduction of the intercalated GO materials [20-25]. Recently, we prepared novel carbon materials containing platinum, ruthenium, or palladium nanoparticles on graphene sheets at ca. 20 wt% from graphite oxide (GO) and metal complexes respectively as $[Pt(NH_3)_4]^{2+}$, $[Ru(NH_3)_6]^{3+}$, or $[Pd(NH_3)_4]^{2+}$ [24]. Their BET surface areas were 400–520 m^2g^{-1}, which were achieved by exfoliated graphene sheets produced using pyrolysis of

precursors having a layer structure like that of intercalation compounds, which were prepared by cation exchange of GO. The respective sizes of platinum, ruthenium, and palladium nanoparticles were 1–3, 1–2, and 3–7 nm. They were dispersed homogeneously on the surface or the space between graphene sheets. It is noteworthy that such materials are producible simply by one-time calcination of the GO-complex precursors, where the exfoliation of GO and deposition of metal nanoparticles occur simultaneously. Furthermore, the amounts and size of metal nanoparticles are controllable using the temperature or the time of heat treatment. They depend also on the degree of oxidation on GO.

We report that graphene sheets having several transition metals such as Au, Ag, Cu, Co, and Ni (Au–Gr, Ag–Gr, Cu–Gr, Co–Gr and Ni–Gr) can be prepared as reported in an earlier paper. Ammine complexes such as $[Cu(NH_3)_4]^+$, $[Co(NH_3)_6]^{3+}$, and $[Ni(NH_3)_6]^{2+}$, bipyridyl complex $[Au(bipy)Cl_2]^+$ (bipy: 2,2'-bipyridyl), and imidazole complex $[Ag(imH)_2]^+$ (imH: imidazole) were used as intercalants to produce the precursors and metal–graphene materials. Results showed that the heat treatment process effects were considerable. Therefore, the effects of the heat treatment procedure on the size distributions of Au and Ag nanoparticles were also investigated. In addition, because Ag nanoparticles are anticipated for use as cathode catalysts for alkaline fuel cells (AFCs), the catalytic activity of Ag–Gr for oxygen reduction reaction (ORR) was measured in KOH aqueous solution in the presence and absence of methanol [26].

2. Experimental

2.1. Materials

According to Brodie's method [27], GO was prepared by oxidation of graphite powder (Wako Pure Chemical Industries Ltd.) using nitric acid and potassium chlorate. The GO composition was estimated as $C_8O_{3.6}H_{2.5\sim3.1}$ using elemental analysis.

Both $[Au(bipy)Cl_2]NO_3$ and $[Ag(imH)_2]NO_3$ were synthesized using procedures described in previous reports [28, 29]. The Au complex of 0.45 g was obtained from 0.65 g 2,2'-bipyridine and 0.80 g $Na[AuCl_4]_2 \cdot H_2O$. The Ag complex of 0.31 g was synthesized from 1.24 g $AgNO_3$ and 2.05 g imidazole.

The $[Cu(NH_3)_4]SO_4$, $[Co(NH_3)_6]Cl_3$, and $[Ni(NH_3)_6]Cl_2$ (Wako Pure Chemical Industries Ltd.) used for this study were used as received.

2.2. Preparation of graphene materials

Au–Gr, Ag–Gr

The GO (0.10 g) was dispersed into a NaOH solution (pH=9.5). After treating the solution under ultrasonic irradiation for 15 min, $[Au(bipy)Cl_2]NO_3$ (0.09 g) was added to the solution. The mixture was stirred for 24 h for ion exchange, and filtered. The obtained compound of Au complex and GO (Au–GO) was heated in an electric furnace under nitrogen atmosphere. Some Au–GO specimens were heated gradually: The specimens were put into a furnace at room temperature; then the furnace temperature was raised to 573 or 523 K at a rate of 5 K min^{-1}. The heating temperature for each compound was determined to achieve good exfoliation of graphene sheets and good nanoparticle dispersion. The specimens were then kept for 30 min at the heating temperature (g-Au–Gr). The other samples were heated rapidly: these specimens were put into a preheated furnace at 573 K, and kept for 10 min at that temperature (r-Au–Gr).

Similarly, samples having Ag were produced by adding $Ag[(imH)_2]NO_3$ (0.10 g) into the GO mixed NH_3 solution at pH=9.5. After stirring and filtering, the compound of Ag complex and GO (Ag–GO) was heated gradually or rapidly in nitrogen atmosphere (*g*-Ag–Gr and *r*-Ag–Gr).

Cu–Gr, Co–Gr and Ni–Gr

The GO (0.20 g) was dispersed into an NH_3 solution (pH=9.5) using ultrasonic irradiation for 15 min. Then $[Cu(NH_3)_4]SO_4$, $[Co(NH_3)_6]Cl_3$, or $[Ni(NH_3)_6]Cl_2$ (0.07 g) was added to the solution and stirred for 24 h. The obtained compounds of Cu, Co, or Ni complexes and GO (Cu–GO, Co–GO, Ni–GO) were calcined gradually by putting them into the furnace at room temperature and then heating them to 673 K at the rate of 5 K min^{-1}. The specimens were kept for 30 min at the heating temperature (Cu–Gr, Co–Gr, Ni–Gr).

2.3. Measurements

The nitrogen adsorption–desorption isotherm was measured at 77 K (Belsorp MAX; Bel Japan Inc.). The BET surface areas and average pore widths were estimated from the isotherms. Powder X-ray diffraction (XRD) patterns were measured using a diffractometer (RINT-2500; Rigaku Corp.) with Cu-Kα radiation. Transmission electron microscope (TEM) images were taken using a microscope (JEM 2100; JEOL). High angular annular dark-field–scanning transmission electron microscopy (HAADF-STEM) images and energy dispersive X-ray spectrometry (EDX) mapping images were obtained for Ni–Gr sample dispersed on a Cu microgrid (Okenshoji Co. Ltd.); they were taken using a microscope (JEM-2100F; JEOL) with a CEOS C_S-corrector for STEM.

The X-ray absorption fine structure (XAFS) spectra were obtained at the BL-9C beamline of the KEK-PF facility (Tsukuba, Japan), which was equipped with a double crystal Si(111) monochromator, under ring operating conditions of 2.5 GeV and 300 mA. The EXAFS data were analyzed using software developed by Maeda [30]. The composition of each sample was inspected using thermogravimetry (TG) analysis in air (MTS9000; Ulvac, Inc.).

The electrochemical measurements for Ag–Gr were conducted in the presence and the absence of methanol at room temperature. Highly pure water, Ag–Gr, and methanol were mixed ultrasonically in an ice bath to prepare the catalyst ink. Then, an aliquot of this ink was dropped onto a glassy carbon disc (GC, 5 mm diameter). After evaporation of the solvent, commercially available Nafion® solution diluted with i-propanol was dropped onto an Ag–Gr loaded GC disk for its use as the working electrode. The electrolyte was 1.0 mol dm^{-3} KOH aqueous solution and/or that and methanol of 1.0 M. A three-electrode cell having Pt mesh as a counter electrode was used. A reversible hydrogen electrode was used as a reference electrode. Linear sweep voltammetry was conducted under nitrogen or oxygen atmosphere with a 1 mV s^{-1} sweep rate using a potentio-galvanostat (ALS-701C; BAS Inc.).

3. Results and Discussion

3.1. BET surface area and nitrogen isotherm

The BET surface area and average pore width ($= 2V/A$, where V is the total pore volume, and A is the surface area) estimated from nitrogen adsorption–desorption isotherms of the samples are presented in Table 1. The temperature at which the exfoliation occurs was different for each compound, meaning that the decomposition of intercalated

cations is significant for the reaction to produce the materials. All samples showed surface areas of 360–620 m^2g^{-1} except Co–Gr (789 m^2g^{-1}). The reason for large surface area of Co–Gr is discussed in a later section. The nitrogen adsorption–desorption isotherms for some samples are portrayed in Figures 1(i)–1(v). Every sample showed a large hysteresis loop, which is attributed to the mesoporous structure. The Au–Gr and Ag–Gr samples showed about 100 ml $(STP)g^{-1}$ of adsorption to micropores, although the other samples (Cu, Co, Ni) had little micropore volume. The micropore sizes of Au–Gr and Ag–Gr were estimated as 0.7 nm using HK analysis.

Table 1

BET surface areas and average pore widths of samples (*g*-Au–Gr, *r*-Au–Gr, *g*-Ag–Gr, *r*-Ag–Gr, Cu–Gr, Co–Gr and Ni–Gr), graphite and GO.

| sample	heating temperature (K)	surface area ($m^2 g^{-1}$)	average pore width (nm)
Graphite	-	5.2	-
GO	-	5.4	-
g-Au–Gr	573	618	5.2
r-Au–Gr	573	505	5.3
g-Ag–Gr	523	504	4.6
r-Ag–Gr	573	565	5.1
Co–Gr	673	789	4.1
Cu–Gr	673	406	7.8
Ni–Gr	673	367	8.5
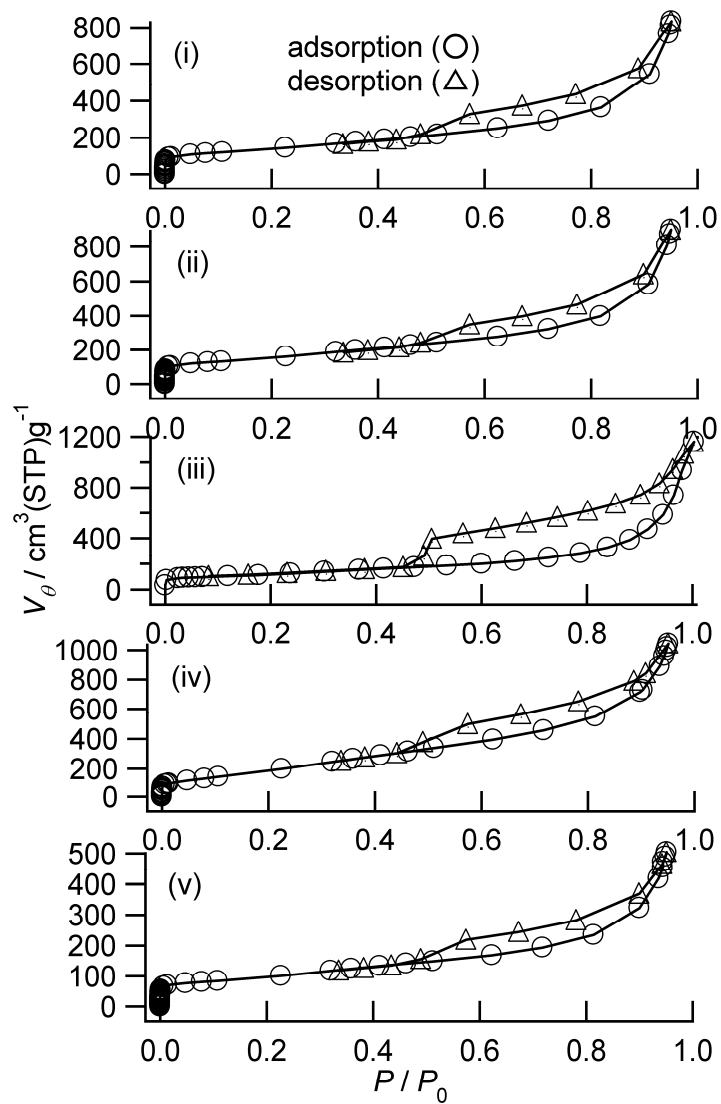
Figure 1. Nitrogen gas adsorption–desorption isotherms of *r*-Au–Gr (i), *r*-Ag–Gr (ii), Cu–Gr (iii), Co–Gr (iv), and Ni–Gr (v).

3.2. X-ray diffraction and Thermogravimetry

Figure 2 shows X-ray diffraction (XRD) patterns of the GO, GO compounds (Au–GO, Ag–GO, Cu–GO, Co–GO, Ni–GO) and heated samples (Au–Gr, Ag–Gr, Cu–Gr, Co–Gr, Ni–Gr). The interlayer distance estimated from the diffraction peak at $2\theta = 13.4°$ was 0.66 nm for GO and was expanded, respectively, to 0.73, 0.72, 0.79, 0.73, and 0.67 nm because of intercalation of each metal complex. Although the other small peaks that were observed could not be attributed completely, they are apparently the peaks of small crystals of metal complex or reduced GO. After heating, the peak disappeared and another broad diffraction of graphite (002) at ca. 24° appeared in each sample, which is attributable to exfoliation of the layer structure and reaggregation of a small part of reduced graphene layers. Diffraction peaks assigned to (111) and (200) of metallic gold were observed for the Au–Gr samples (Figure 2(i) *g-*Au–Gr and *r-A*u–Gr). The crystallite size of Au metal calculated from the peaks using Scherrer's equation were, respectively, ca. 8 and 5 nm for *g-*Au–Gr and *r-*Au–Gr. The Ag–Gr sample also showed peaks of (111) and (200) reflection of Ag metal (Figure 2(i)). The calculated crystallite sizes of the Ag in *g-*Ag–Gr and *r-*Ag–Gr were, respectively, ca. 18 and 12 nm. However, (002) and (100) diffraction peaks of cupric oxide (CuO) were observed for the Cu–Gr sample (Figure 2(ii)). The crystallite size of CuO was estimated at 5 nm. The Co–Gr sample had no diffraction peaks of metal and metal oxide (Figure 2(ii)). Regarding Ni–Gr, the XRD pattern had diffraction peaks of both nickel metal ($2\theta = 44.5°$) and nickel oxide ($2\theta = 43.6°$) (Figure 2(ii)). The crystallite size of Ni metal was estimated at 22 nm, although the reflection by nickel oxide was too weak to estimate the crystallite size. The chemical states of cobalt in Co–Gr and nickel in Ni–Gr are also discussed in the following paragraphs.

The loading amounts of Au and Ag in *g*-Au–Gr and *r*-Ag–Gr samples were estimated respectively as 13.3 wt.% and 14.0 wt.% using thermogravimetric (TG) measurements in air. Estimations for those of Cu, Co, and Ni were difficult because of the weight change attributable to metallic oxide formation. However, the amount for each sample was calculated roughly as about 5–10% from the increase in the weight by ion-exchange of GO.
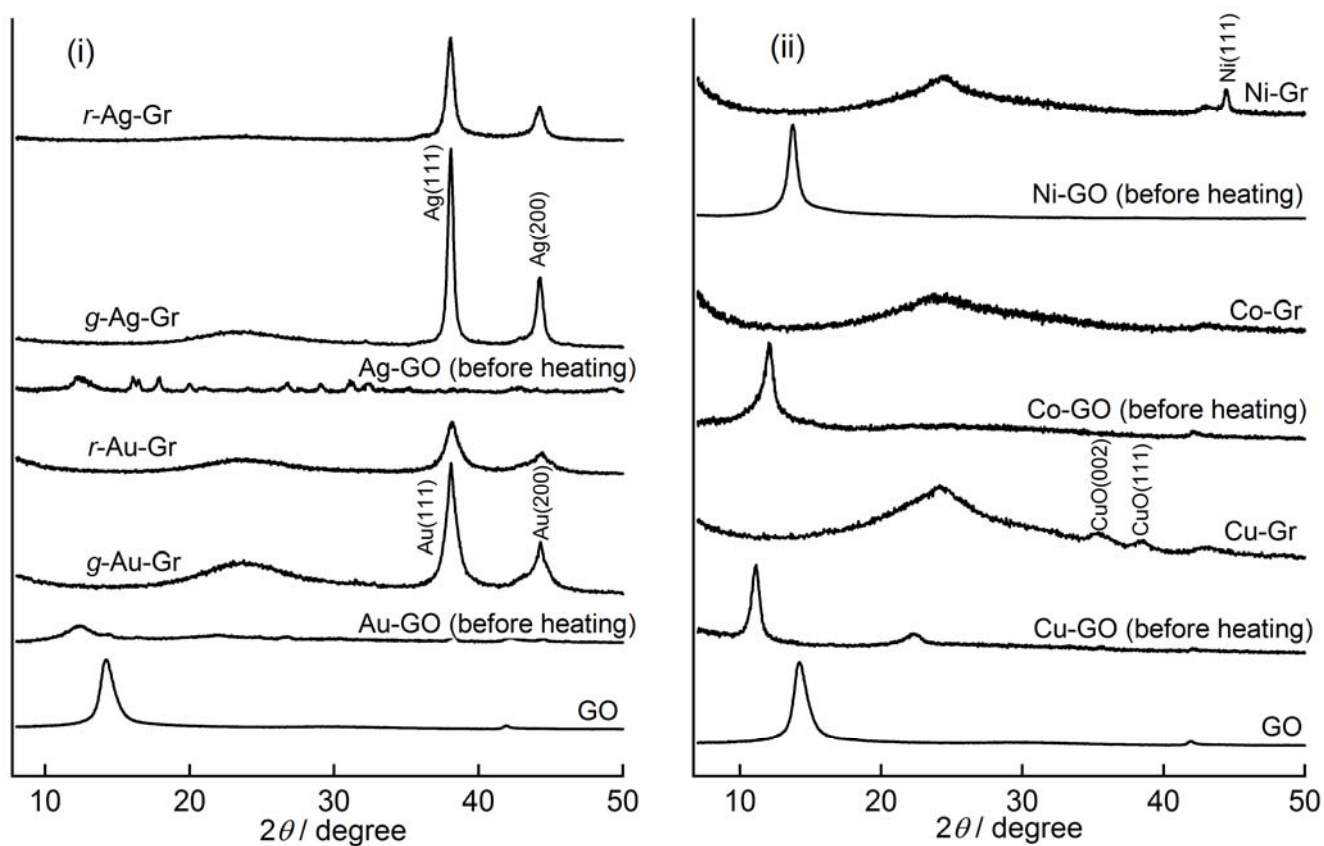

Figure 2. X-ray diffraction (XRD) patterns of GO, intercalated compounds (before heating), and heated samples. The respective heating temperatures for samples coincide with those of the samples in Table 1 (*g*-Au–Gr, *r*-Au–Gr, *g*-Ag–Gr, *r*-Ag–Gr, Cu–Gr, Co–Gr, and Ni–Gr).

3.3. TEM images and XAFS spectra

Some TEM images of Au–Gr and Ag–Gr samples are portrayed in Figures 3(i)–3(iv). These consist of exfoliated graphene sheets and metal nanoparticles; they resemble the images of Pt, Pd, or Ru samples that we reported [24]. No micropore or mesopore was observed on the carbon surface. Therefore, the mesoporous structure estimated by isotherm measurement is attributable to the space between exfoliated graphene sheets and/or the void in wrinkled parts on graphene sheets. A microporous structure observed using isotherm measurements is explainable by the space at the intrametal or intermetal nanoparticles, and/or between graphene and metal nanoparticles. The Au particle size distribution estimated from the TEM images is shown in Figures 4(i) and 4(ii). The gradually heated sample, *g*-Au–Gr (Figure 4(i)), had smaller particles of less than 5 nm and some larger particles (10–20 nm), but the rapidly heated sample, *r*-Au–Gr (Figure 4(ii)), has larger average particle size than *g*-Au–Gr. Nevertheless, few particles larger than 15 nm were observed. That result shows good agreement with the estimation from XRD peaks by considering a contribution of large particles of Au metal. In fact, Ag–Gr has a similar distribution to that of Au–Gr (Figures 4(iii) and 4(iv)). The average particle size for the gradually heated sample, *g*-Ag–Gr (Figure 4(iii)), is smaller than that of the rapidly heated sample, *r*-Ag–Gr (Figure 4(iv)), although some huge Ag particles larger than 35 nm were observed. In both Au and Ag samples, smaller particles of less than 1 nm were also observed, which were not included in Figure 4 because of the difficulty in measuring the size precisely. Based on the TEM observation, it can be interpreted that brief heat treatment (about 10 min) is preferred to mitigate the formation of particles larger than 15 nm.
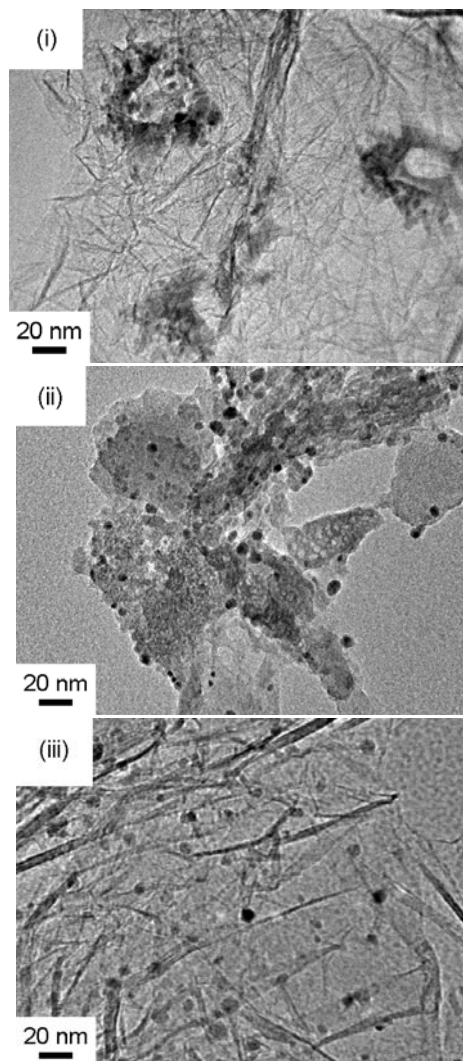
The TEM images of Cu–Gr, Co–Gr, and Ni–Gr samples are depicted respectively in Figures 5(i), 5(ii), and 5(iii). Nanoparticles on graphene were also observed in these samples. The sizes of nanoparticles are distributed between 2–9 nm for each sample. The particles in Cu–Gr sample aggregated and produced some colonies on exfoliated graphene sheets. It is apparently midway through aggregation to large CuO particles, reported by Kyotani et al. [20]. Particles in Ni–Gr were distributed inhomogeneously: both well-dispersed areas and aggregated areas were observed. In contrast, particles in Co–Gr dispersed homogeneously throughout the carbon sheets, but the graphene sheets had a vermiculate shape, which is attributable to the origin of high surface areas on the Co–Gr material.
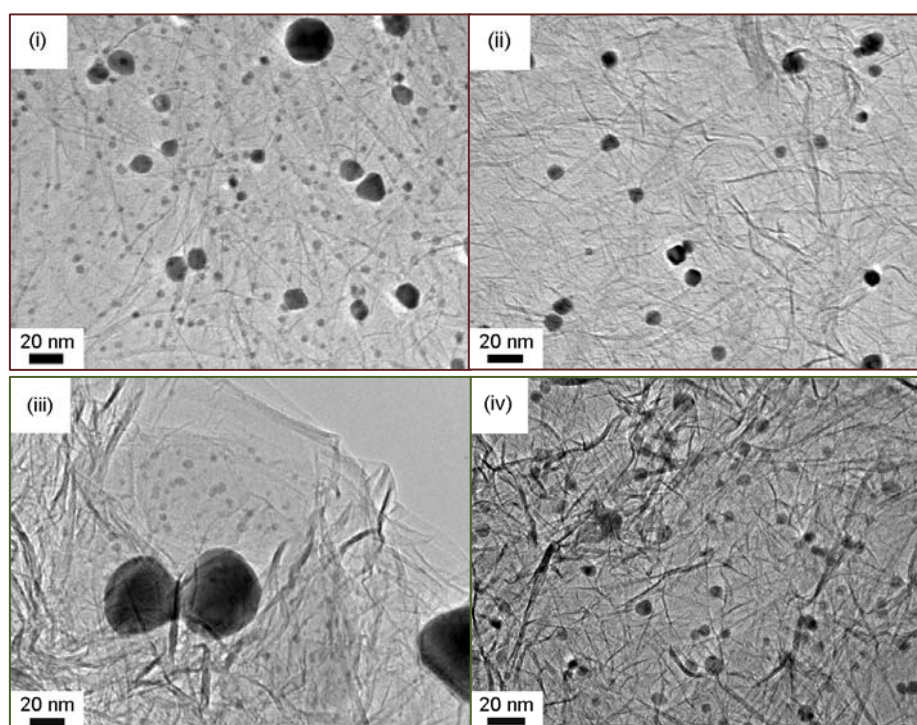
Figure 3. TEM images of *g*-Au–Gr heated at 573 K (i), *r*-Au–Gr heated at 573 K (ii), *g*-Ag–Gr heated at 523 K (iii), and *r*-Ag–Gr heated at 573 K (iv).
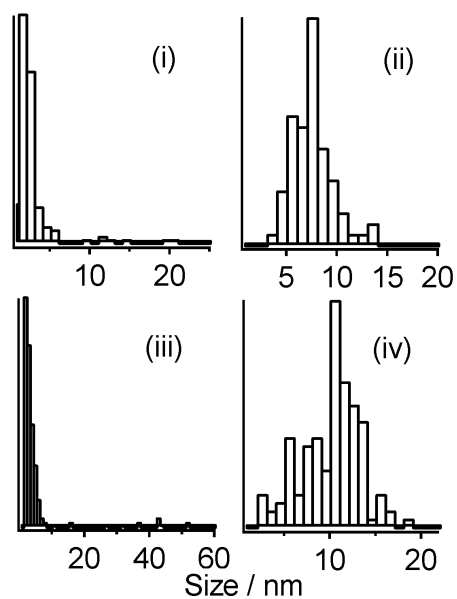
Figure 4. Distributions of Au and Ag particle sizes in *g*-Au–Gr heated at 573 K (i), *r*-Au–Gr heated at 573 K (ii), *g*-Ag–Gr heated at 523 K (iii), and *r*-Ag–Gr heated at 573 K (iv).

Figure 5. TEM images of Cu–Gr heated at 673 K (i), Co–Gr heated at 673 K (ii), and Ni–Gr heated at 673 K (iii).

Figure 6 portrays EXAFS and XANES spectra of Co–Gr and Co foil. The spectra of Co–Gr differed greatly from those of Co foil. Moreover, the Co–Gr sample had a peak of magnitude in the EXAFS spectrum (Figure 6(i)) at 0.14 nm (the scale of distance in (i) is that of no phase correction), which should be assigned to the bond distance between Co and O. The bond distance of Co–Co was shorter by 0.22 nm than that observed for Co foil [31]. The peak at ca. 7.723 keV of Co–Gr in XANES (Figure 6(ii)) spectra suggests that the cobalt oxide composition is CoO [32, 33].

Figure 7 displays an HAADF-STEM image (i), a part of an HAADF-STEM image (ii) and EDX maps at the same area for Ni and O atoms in Ni–Gr. Several sizes of nickel particles between 0.5–80 nm were observed on carbon sheets. The spots of two-dimensional Fourier transformation image for the particle in the center of Figure 7(ii) showed the d values of 0.211 and 0.185 nm, which almost correspond respectively to (111) and (200) planes of Ni metal. Oxygen was observed not only on the graphene sheets but also on the surface of larger Ni-particles in the EDX map (Figure 7(iii)). The density of oxygen in smaller particles and in the inner area of larger particles is lower than that on the surface, which indicates that most Ni particles in Ni–Gr were metal, but that the surfaces of large particles were partly oxidized, forming a core–shell structure. However, many extremely tiny Ni particles smaller than 0.18 nm were also observable on the surface of graphene sheets in the HAADF-STEM image (Figure 7(ii)). The surface composition of nanoparticles and the state of the tiny particles are expected to affect the activity for catalytic reaction. Examination of some organic reactions using these samples as a catalyst is in progress. The results will be reported in the near future.
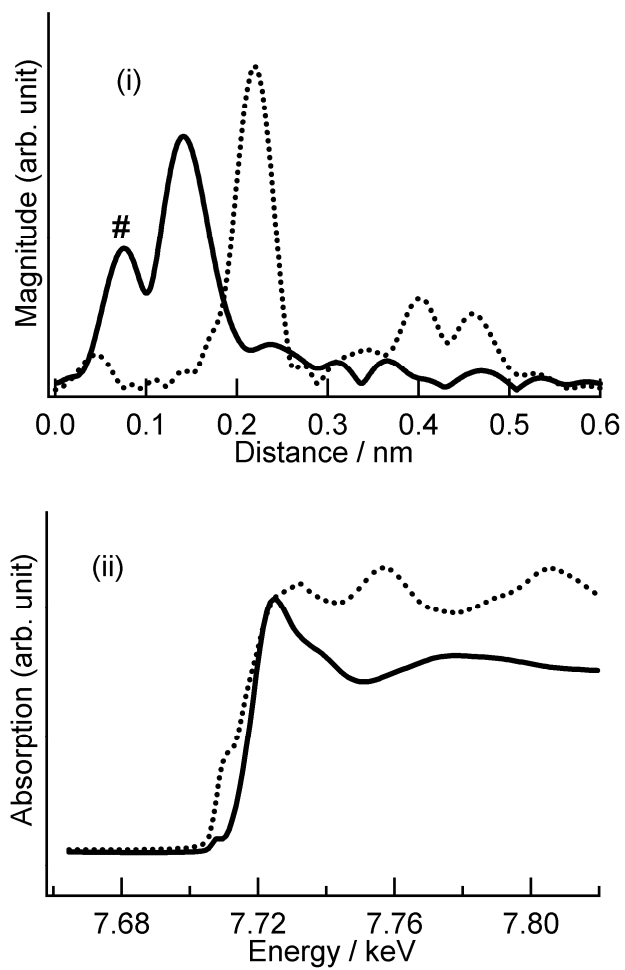
Figure 6. EXAFS (i) and XANES spectra (ii) of Co–Gr sample (solid line) and Co foil (dotted line). The scale of distance in (i) is in no phase correction. The peak marked with # is a ghost.
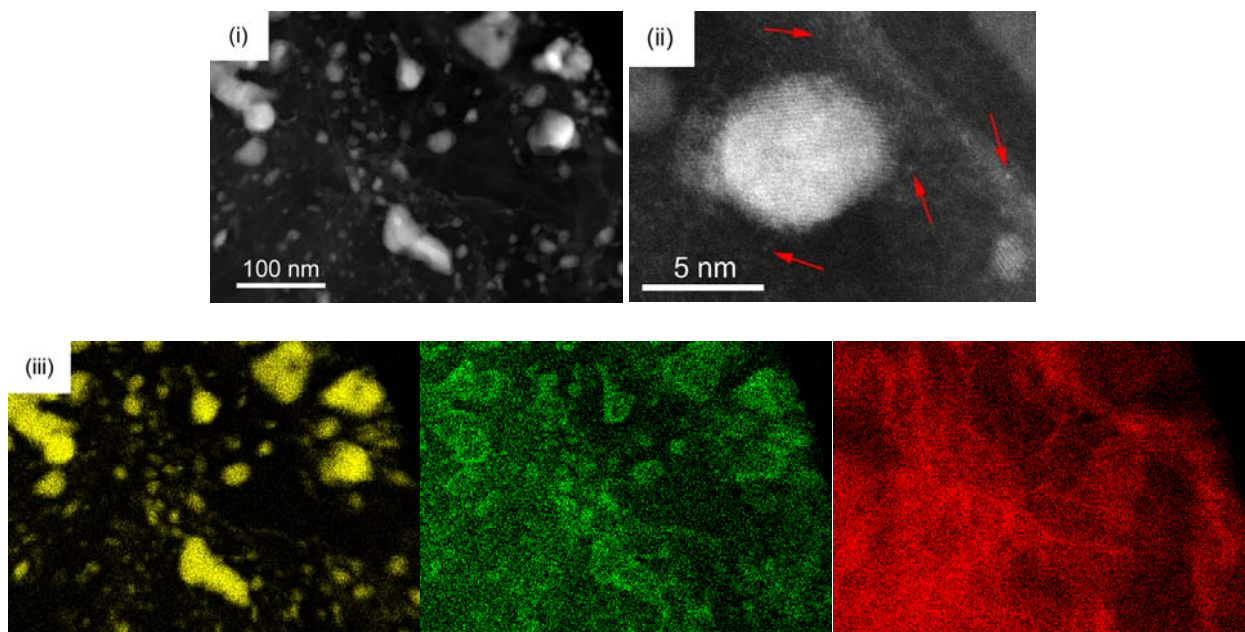
Figure 7. HAADF-STEM image (i), a part of an HAADF-STEM image (ii), and EDX maps of an HAADF-STEM image for Ni (iii, yellow), O (iii, green), and C (iii, red) atoms in a Ni–Gr sample. Some extremely tiny Ni particles (smaller than 0.18 nm) in (ii) are indicated by red arrows.

3.4. Electrochemical analysis for Ag-graphene

Catalytic activity for ORR of *r*-Ag–Gr was investigated. Linear sweep voltammograms (LSV) are presented in Figure 8. Figure 8(a) shows the LSVs in 1.0 KOH aq in the absence of methanol under nitrogen (black broken line) and oxygen (red solid line) atmospheres. Under a nitrogen atmosphere, no faradic current was observed; in contrast, under an oxygen atmosphere, the reduction current was observed below ca. 0.81 V *vs*. RHE, which proves that Ag–Gr has ORR activity in the alkaline solution. Therefore Ag–Gr prepared in this study is promising for use as a novel cathode catalyst of AFCs. Similar results were obtained for the presence of methanol at 1.0 M (Figure 8(b)). In particular, the onset potential for ORR exists irrespective of the presence of methanol, which could be a feature for Ag–Gr.

Results show that Ag–Gr is promising as a novel cathode catalyst not only for use in AFCs but also in AFCs employing alcohol as fuel (direct alcohol alkaline fuel cells: DAAFCs). The most important feature of Ag–Gr is considered to be its higher catalyst utility than that of conventional carbon materials (activated carbon). Results show a unique structure by which metal catalysts on the thin carbon sheets can react with oxygen. It presents important advantages for construction of a triple-phase boundary. To prove this, further study such as that of fuel cell tests is necessary for Ag–Gr.
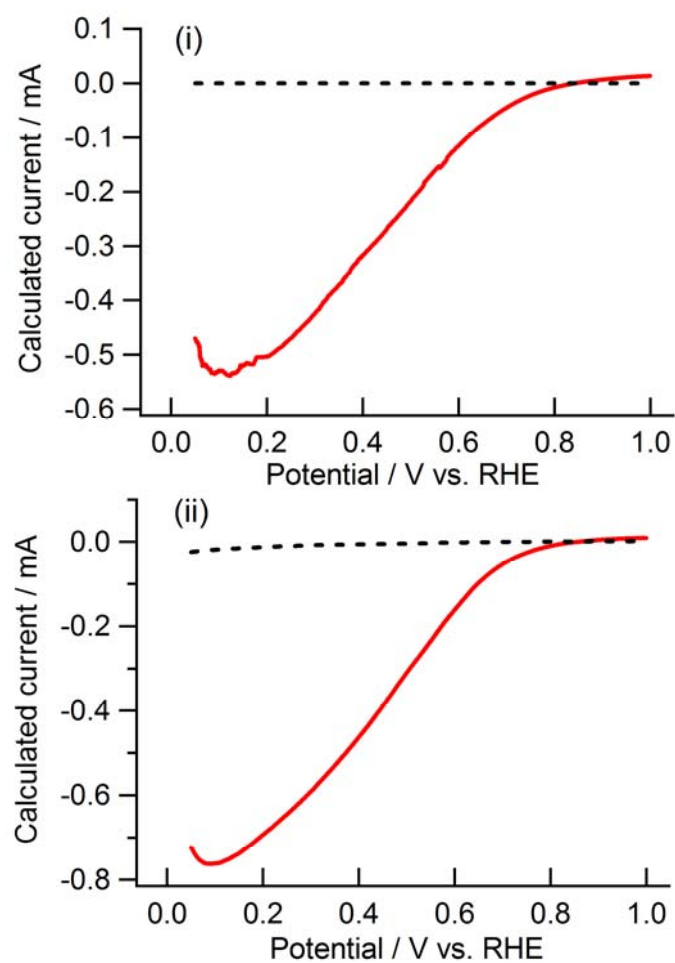
Figure 8. Linear sweep voltammograms (LSVs) of Ag–Gr in 1.0 KOH aq. (i) and Ag–Gr in 1.0 M MeOH – 1.0 KOH aq. (ii) under oxygen atmosphere (red solid line) or nitrogen atmosphere (black broken line).

4. Conclusion

A heating method to produce Pt-carbon, Ru-carbon, and Pd-carbon was applied to production of graphene sheets supporting Au, Ag, Cu, Co, or Ni. The materials were produced from ion-exchanged GOs, which include cations of ammine complexes, 2,2'-bipyridyl complex, or imidazole complex. Each sample consists of exfoliated graphene sheets and supported metal or metal oxide nanoparticles. The Au in Au–Gr and Ag in Ag–Gr samples existed as metal nanoparticles, whereas Cu in Cu–Gr and Co in Co–Gr were observed as metal oxides using XRD, XANES, and EXAFS. Most Ni particles in Ni–Gr were metal, but the surfaces of large particles were partly oxidized, as revealed by HAADF-STEM and EDX mapping of STEM measurements. The size distribution of Au in Au–Gr and Ag in Ag–Gr was controllable by the heat treatment conditions. The Ag–Gr sample showed catalytic activity for ORR in 1.0 M KOH aq. under an oxygen atmosphere. The presence of methanol did not disturb the reduction.

In the present report and in a previous report [24], we described a series of carbon materials consisting of graphene sheets and metal nanoparticles from cation exchanged GOs, showing that some were useful as catalysts. Application to other chemical (organic or inorganic) and electrochemical reactions using these samples as catalysts is also anticipated.

References

[1]   Park S, Ruoff RS. Chemical methods for the production of graphenes. Nature Nanotech 2009;4(4):217–24.

[2]   Choi W, Lahiri I, Seelaboyina R, Kang YS. Synthesis of graphene and its applications. Crit Rev Solid State Mater Sci 2010;35(1):52–71.

[3]   Compton OC, Nguyen ST. Graphene oxide, highly reduced graphene oxide, and graphene: versatile building blocks for carbon-based materials. Small 2010;6(6):711–23.

[4]   Dreyer DR, Park S, Bielawski CW, Ruoff RS. The chemistry of graphene oxide. Chem Soc Rev 2010;39(1):228–40.

[5]   Shen J, Hu Y, Shi M, Lu X, Qin C, Li C et al. Fast and facile preparation of graphene oxide and reduced graphene oxide nanoplatelets. Chem Mat 2009;21(15):3514–20.

[6]   Schniepp HC, Li JL, McAllister MJ, Sai H, Herrera-Alonso M, Adamson DH et al. Functionalized single graphene sheets derived from splitting graphite oxide. J Phys Chem B 2006;110(17):8535–9.

[7]   Du Q, Zheng M, Zhang L, Wang Y, Chen J, Xue L et al. Preparation of functionalized graphene sheets by a low-temperature thermal exfoliation approach and their electrochemical supercapacitive behaviors. Electrochim Acta 2010;55(12):3897–903.

[8]   Lv W, Tang DM, He -B, You CH, Shi ZQ, Chen XC et al. Low-Temperature Exfoliated Graphenes: Vacuum-Promoted Exfoliation and Electrochemical Energy Storage. ACS Nano 2009;3(11):3730–6.

[9]   Rao CNR, Biswas K, Subrahmanyam KS, Govindaraj A. Graphene, the new nanocarbon. J Mater Chem 2009;19(17):2457–69.

[10]   Liang MH, Luo B, Zhi LJ. Application of graphene and graphene-based materials in clean energy-related devices. Int J Energy Res 2009;33(13):1161–70.

[11]   Lightcap IV, Kosel TH, Kamat PV. Anchoring Semiconductor and Metal Nanoparticles on a Two-Dimensional Catalyst Mat. Storing and Shuttling Electrons with Reduced Graphene Oxide. Nano Letters 2010;10(2):577–83.

[12]   Zhang X-Y, Li H-P, Cui X-L, Lin Y. Graphene/TiO2 nanocomposites: synthesis, characterization and application in hydrogen evolution from water photocatalytic splitting. J Mater Chem 2010;20(14):2801–6.

[13]   Liu Y-J, Wang Z-M, Aizawa M, Peng W-Q, Hirotsu T. Nanoporous composite of carbon nanosheets and functional titania nanoparticles formed by reassembling of exfoliated graphite oxides with colloidal titania. Mater Lett 2009;63(2):260–2.

[14]   Kamat PV. Graphene-based nanoarchitectures. Anchoring semiconductor and metal nanoparticles on a two-dimensional carbon support. J Phys Chem Lett 2010;1(2):520–7.

[15]   Kou R, Shao Y, Wang D, Engelhard MH, Kwak JH, Wang J et al. Enhanced activity and stability of Pt catalysts on functionalized graphene sheets for electrocatalytic oxygen reduction. Electrochem Commun 2009;11(5):954–7.

[16]   Dong L, Gari RRS, Li Z, Craig MM, Hou S. Graphene-supported platinum and platinum–ruthenium nanoparticles with high electrocatalytic activity for methanol and ethanol oxidation. Carbon 2010;48(3):781–7.

[17]   Shao Y, Zhang S, Wang C, Nie Z, Liu J, Wang Y et al. Highly durable graphene nanoplatelets supported Pt nanocatalysts for oxygen reduction. J Power Sources 2010;195(15):4600–5.

[18]   Li Y, Gao W, Ci L, Wang C, Ajayan PM. Catalytic performance of Pt nanoparticles on reduced graphene oxide for methanol electro-oxidation. Carbon 2010;48(4):1124–30.

[19]   Liu S, Wang J, Zeng J, Ou J, Li Z, Liu X et al. "Green" electrochemical synthesis of Pt/graphene sheet nanocomposite film and its electrocatalytic property. J Power Sources 2010;195(15):4628–33.

[20]   Kyotani T, Suzuki K, Yamashita H, Tomita A. Formation of carbon-metal composites from metal ion exchanged graphite oxide. Tanso 1993;160:255–65.

[21]   Morishige K, Hamada T. Iron oxide pillared graphite. Langmuir 2005;21(14):6277–81.

[22]   Mastalir Á, Király Z, Patzkó Á, Dékány I, L'Argentiere P. Synthesis and catalytic application of Pd nanoparticles in graphite oxide. Carbon 2008;46(13):1631–7.

[23]   Afanasov IM, Shornikova ON, Avdeev VV, Lebedev OI, Van Tendeloo G, Matveev AT. Expanded graphite as a support for Ni/carbon composites. Carbon 2009;47(2):513–8.

[24]   Gotoh K, Kawabata K, Fujii E, Morishige K, Kinumoto T, Miyazaki Y et al. The use of graphite oxide to produce mesoporous carbon supporting Pt, Ru, or Pd nanoparticles. Carbon 2009;47(8):2120–4.

[25]   Hu ZL, Aizawa M, Wang ZM, Hatori H. Palladium precursor for highly efficient preparation of carbon nanosheet-palladium nanoparticle composites. Carbon 2009;47(14):3377–80.

[26]   Antolini E, Gonzalez ER. Alkaline direct alcohol fuel cells. J Power Sources 2010;195(11):3431–50.

[27]   Nakajima T, Matsuo Y. Formation process and structure of graphite oxide. Carbon 1994;32(3):469–75.

[28]   Harris CM, Lockyer TN. Nitrogenous chelate complexes of transition metals. II. The trivalent gold complexes of 2,2'-bipyridyl. J Chem Soc 1959;3083–5.

[29]   Antti CJ, Lundberg BKS. The molecular and crystal structure of diimidazole silver(I) nitrate, Ag(C3H4N2)2NO3. Acta Chem Scand 1971;25(5):1758–66.

[30]   Maeda H. Accurate bond length determination by EXAFS method. J Phys Soc Jpn 1987;56(8):2777–87.

[31]   Liu XC, Shi EW, Chen ZZ, Chen BY, Huang W, Song LX et al. The local structure of Co-doped ZnO films studied by X-ray absorption spectroscopy. J Alloys Compounds 2008;463(1-2):435–9.

[32]   Jacobs G, Ji Y, Davis BH, Cronauer D, Kropf AJ, Marshall CL. Fischer–Tropsch synthesis: Temperature programmed EXAFS/XANES investigation of the influence of support type, cobalt loading, and noble metal promoter addition to the reduction behavior of cobalt oxide particles. Applied Catal A 2007;333(2):177–91.

[33]   Khemthong P, Klysubun W, Prayoonpokarach S, Wittayakun J. Reducibility of cobalt species impregnated on NaY and HY zeolites. Mat Chem Phys 2010;121(1–2):131–7.